ELSEVIER

Journal of Alloys and Compounds 446–447 (2007) 271–275

Journal of ALLOYS AND COMPOUNDS

www.elsevier.com/locate/jallcom

Kinetics and thermodynamics of the aluminum hydride polymorphs

J. Graetz [a,*], J.J. Reilly [a], J.G. Kulleck [b], R.C. Bowman [b]

[a] *Department of Energy Sciences and Technology, Brookhaven National Laboratory, Upton, NY 11973, USA*
[b] *Jet Propulsion Laboratory, California Institute of Technology, Pasadena, CA 91109, USA*

Received 25 September 2006; accepted 30 November 2006
Available online 29 December 2006

Abstract

Polymorphs of AlH_3 were prepared by organometallic synthesis. We demonstrate that freshly synthesized, nonsolvated AlH_3 releases approximately 10 wt% H_2 at desorption temperatures less than 100 °C. The decomposition kinetics, measured by isothermal hydrogen desorption between 30 and 140 °C, suggest that the rate of H_2 evolution is limited by nucleation and growth of the aluminum phase. The H_2 evolution rates for small crystallites of α and γ-AlH_3 (undoped) meet the DOE full flow target for a 50 kW fuel cell (1 gH_2/s) above 114 °C (based on 100 kg AlH_3). The decomposition thermodynamics were measured using differential scanning calorimetry and ex situ X-ray diffraction. The decomposition of the less stable polymorph, γ-AlH_3, occurs by an exothermic transformation to the α phase (∼100 °C) followed by the decomposition of α-AlH_3. A formation enthalpy of approximately −10 kJ/mol AlH_3 was measured for α-AlH_3, which is in good agreement with previous experimental and calculated results.

Keywords: Energy storage materials; Hydrogen storage materials; Thermal analysis; Calorimetry

1. Introduction

Aluminum hydride, or alane (AlH_3), is potentially an attractive storage material due to the large amount of hydrogen that can be contained in a relatively small, lightweight package. AlH_3 contains 10% H by weight and has a theoretical H density of 148 g/L, which is more than double the density of liquid H_2. AlH_3 exhibits seven different known polymorphs [1]. Each phase has a unique structure and atomic arrangement and therefore exhibits different thermodynamic and kinetic properties. Thermodynamic studies of the α phase suggest equilibrium H_2 pressure of around 10^5 bar at 298 K [2,3]. Therefore, α-AlH_3, and the other less stable polymorphs, can spontaneously decompose at room temperature. However, due apparently to the presence of a stabilizing surface layer, early experiments on AlH_3 synthesized by the DOW Chemical Company exhibited slow H_2 evolution rates below 150 ° C. Sandrock et al. have demonstrated that the addition of a dopant, LiH, introduced by ball milling, alters this surface barrier and lowers the decomposition temperature by 25–50 °C [4,5]. More recently, freshly synthesized nanoscale AlH_3 has been shown to decompose at less than 100 °C without the need of a dopant or ball milling [6]. In addition, the total H_2 yield with the fresh material approaches the theoretical value of 10 wt%.

2. Methods

Calorimetric measurements were performed using a Mettler Toledo DSC822^e differential scanning calorimeter (DSC) using a dynamic temperature ramp between 35 and 300 °C at a rate of 10 °C/min. X-ray powder diffraction (XRPD) experiments were performed using Cu Kα radiation. XRPD samples were coated with silicon-based vacuum grease and sealed under a Kapton film to prevent air exposure. Crystallite sizes were estimated from surface area measurements based on spherical particle geometry. Surface area measurements were performed with a Quanta Chrome NOVA 1000 surface area analyzer on the decomposed material (Al powder) after a 10 h degassing procedure at 200 °C. Isothermal desorption measurements were performed by heating approximately 0.33 g of AlH_3 in an evacuated volume ($V \approx 1.2$ L). The sample temperature was measured with internal and external thermocouples. Sample handling, transfer, and storage were performed under an inert atmosphere in a purified Ar glovebox.

3. Materials

The alane samples used in this study were prepared by an ethereal reaction of $AlCl_3$ with $LiAlH_4$ originally developed by Brower et al. [1]:

$$3LiAlH_4 + AlCl_3 \xrightarrow{Et_2O} 3LiCl + 4AlH_3 \cdot Et_2O \quad (1)$$

The LiCl precipitate is removed by filtration to yield a solution of etherated aluminum hydride, $AlH_3{\cdot}[C_2H_{52}O]$. Stabilized α-AlH_3, consisting of large

* Corresponding author.
E-mail address: graetz@bnl.gov (J. Graetz).

0925-8388/$ – see front matter © 2006 Elsevier B.V. All rights reserved.
doi:10.1016/j.jallcom.2006.11.205

cuboid crystallites (~50 μm), was prepared by the Dow Chemical Company using a continuous crystallization method. In this process, the aluminum hydride etherate, formed in Eq. (1), is used as a feed solution and added to a crystallization medium of benzene, ether, and a selection of complex metal hydrides at ~77 °C [1]. This material is completely inert in air, which is likely attributed to a small amount of organic material incorporated into the surface as a protective coating [7,8]. A scanning electron microscopy (SEM) micrograph of a single crystallite is shown in Fig. 1(a) and the XRPD pattern from the large crystallite batch is shown in Fig. 1(b).

Small crystallites of α-AlH_3 were freshly prepared by heating AlH_3 etherate (formed by reaction (1)) in the presence of a complex metal hydride ($LiAlH_4$ and $LiBH_4$) under a reduced atmosphere for up to four hours. A surface area of 11 m^2/g was measured by BET, suggesting a particle diameter of ~200 nm (based on a spherical geometry). The SEM micrograph and associated XRPD pattern are shown in Figs. 1(c) and (d). The XRPD pattern is nearly identical to that of Fig. 1(b) with the exception of a much smaller (0 1 2) Bragg peak ($2\theta = 28°$) relative to the other Bragg reflections. This is due to the smaller particle size, which allows for better averaging over all crystallite orientations.

A similar procedure was used to form small crystallites of γ-AlH_3. The AlH_3 etherate (formed by reaction (1)) was heated at 65 °C in the presence of $LiAlH_4$. A surface area of 16 m^2/g was measured by BET, suggesting a particle diameter of ~140 nm (based on a spherical geometry). The SEM micrograph and associated XRPD pattern from γ-AlH_3 are shown in Figs. 1(c) and (d). It is interesting to note that at this scale the particle morphology appears similar to that of the small crystallites of α-AlH_3 (Fig. 1(c)).

4. Decomposition pathway and thermodynamics

The decomposition of α-AlH_3 occurs in a single endothermic reaction:

$$\alpha\text{-}AlH_3 \rightarrow Al + 3/2H_2 \quad (2)$$

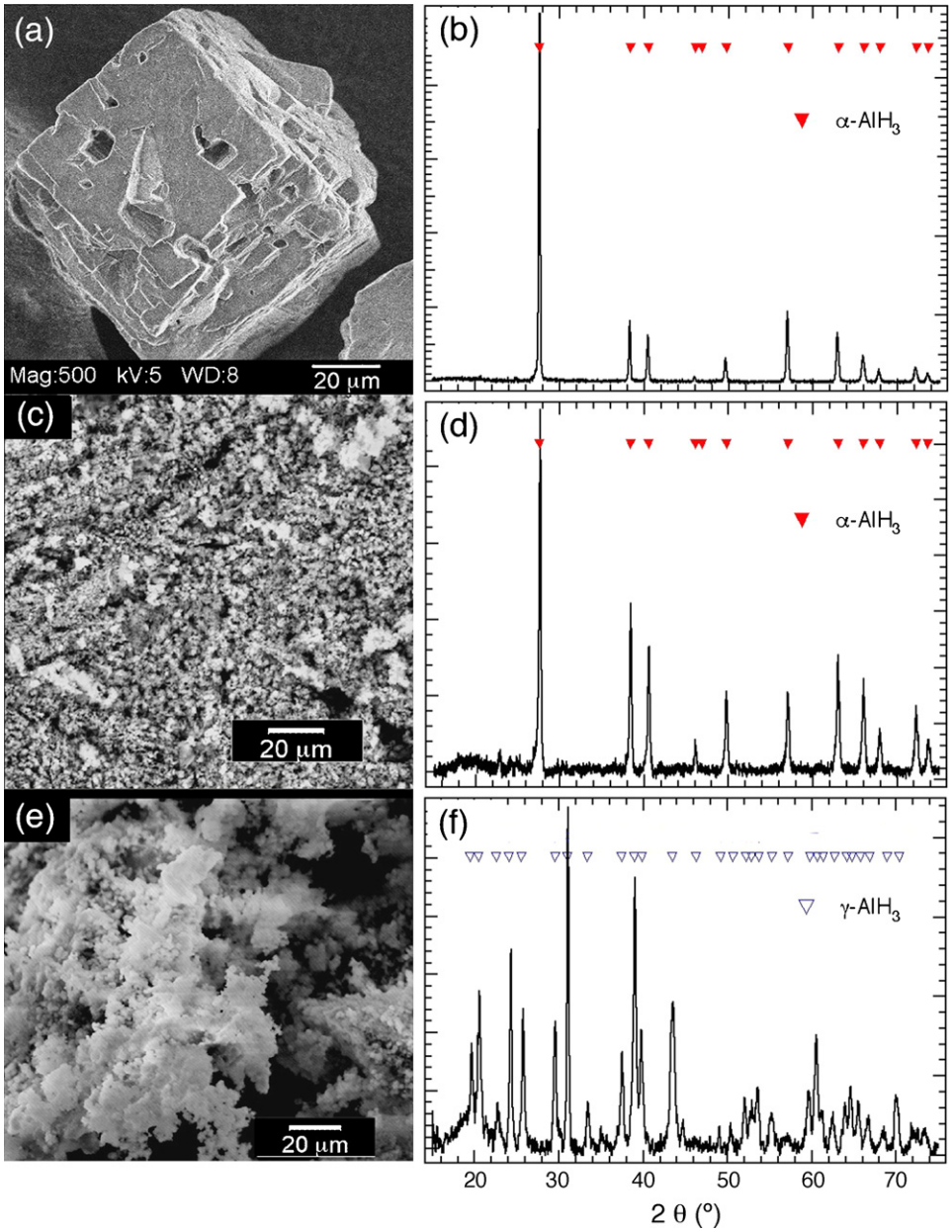

Fig. 1. SEM micrographs and X-ray diffraction patterns from (a, b) α-AlH_3 prepared by Dow Chem. Co. (c, d) α-AlH_3 prepared by BNL, and (e, f) γ-AlH_3 prepared by BNL.

The decomposition of the stabilized (50 μm) and freshly synthesized (200 nm) α-AlH_3 are shown in the DSC traces in Fig. 2(I) and (III), respectively. The stabilized material exhibits an endotherm at ∼210 °C due to decomposition (reaction (2)) and a small exothermic peak at ∼230 °C possibly due to a reaction with surface impurities. The freshly prepared, small crystallites of α-AlH_3 exhibit a decomposition endotherm at ∼170 °C (reaction (2)). The reduced decomposition temperature is attributed to a clean surface and smaller crystallite size. Based on calorimetric data from the freshly prepared material, the enthalpy (ΔH_f) and Gibbs free energy (ΔG_f) for the formation of α-AlH_3 are $\Delta H = -9.9$ kJ/mol AlH_3 and $\Delta G_{f298\,K} = 46.4$ kJ/mol AlH_3, respectively [3]. These values are consistent with those of Sinke et al.: $\Delta H_f = -11.4 \pm 8$ kJ/mol AlH_3 and $\Delta G_{f298\,K} = 46.4 \pm 11$ kJ/mol AlH_3 [9]. The insets of Fig. 2 show the atomic structure before (α-AlH_3 : $R\bar{3}c$) and after decomposition (Al : $Fm\bar{3}m$). Although the unit cell contracts by approximately 50% (AlH_3: 20 cm^3/mol; Al: 10 cm^3/mol), the geometry of the Al atoms does not change during decomposition [10].

The DSC trace from γ-AlH_3 is shown in Fig. 2(II). The exothermic peak at ∼110 °C is attributed to a phase transition to the α polymorph. The γ → α transition enthalpy is $\Delta H_{\gamma-\alpha} = -2.8 \pm 0.4$ kJ/mol AlH_3 [3]. The endotherm at ∼170 °C is due to the decomposition of the α phase (reaction (2)) and the enthalpy is similar to that measured for the pure α phase (−9.9(6) kJ/mol AlH_3). The transition exotherm does not overlap the decomposition endotherm, suggesting that for high

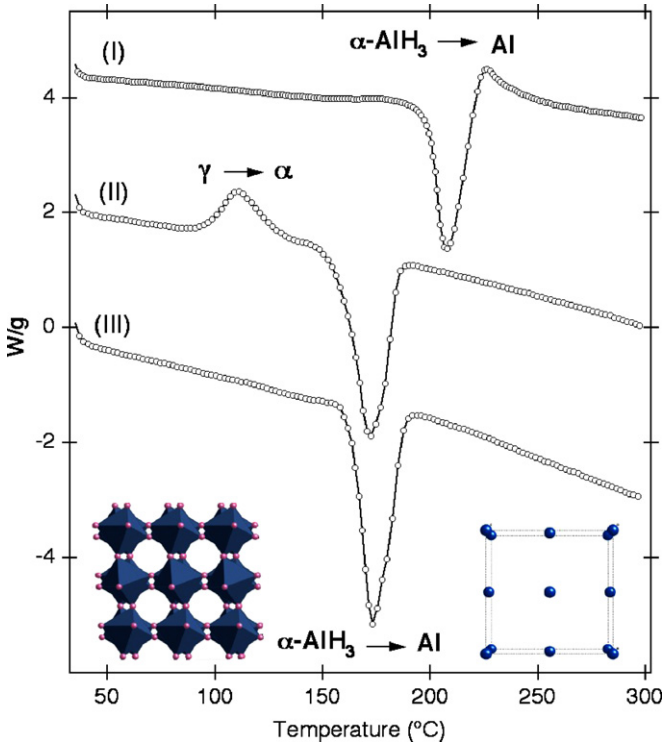

Fig. 2. Differential scanning calorimetry of (I) large crystallites of α-AlH_3 (Dow), (II) small crystallites of γ-AlH_3, and (III) small crystallites of α-AlH_3. The insets show the atomic structure of α-AlH_3 before (α-AlH_3 : $R\bar{3}c$) and after decomposition (Al : $Fm\bar{3}m$).

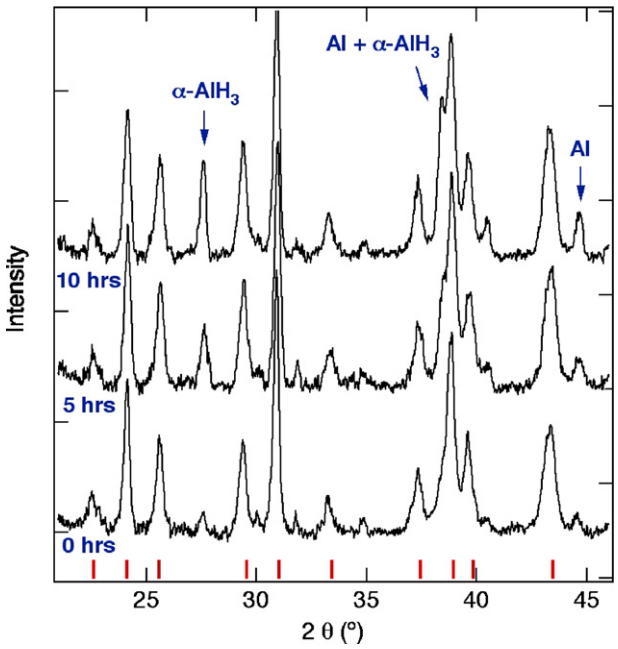

Fig. 3. Ex situ X-ray powder diffraction patterns from γ-AlH_3 at 60 °C showing an increase in α-AlH_3 and Al metal. The dashed markers (|) indicate the peak positions for γ-AlH_3.

temperatures (≥100 °C) and rapid heating rates (≥10 °C/min) the decomposition of γ-AlH_3 occurs in two steps:

$$\gamma\text{-}AlH_3 \rightarrow \alpha\text{-}AlH_3 \rightarrow Al + 3/2H_2\ (T \geq 100\,^{\circ}C) \quad (3)$$

At temperatures below 100 °C the reaction is more complicated. Ex situ XRPD from γ-AlH_3 (Fig. 3) reveal an increase in the concentration of both Al metal and α-AlH_3 over a 10 h period at 65 °C. Recent kinetic and thermodynamic studies [6,11] suggest that at low temperature (≤100 °C) two decomposition pathways are present for γ-AlH_3: (1) direct decomposition to the elements (γ-$AlH_3 \rightarrow Al + 3/2H_2$) and (2) a phase transformation to the α polymorph followed by decomposition of the α phase (γ-$ALH_3 \rightarrow$ α-$ALH_3 \rightarrow Al + 3/2H_2$). The existence of two decomposition pathways at low temperature is also supported by recent ^{27}Al and proton NMR results [12].

5. Hydrogen evolution rates

AlH_3 samples were decomposed isothermally into an evacuated volume ($V \approx 1.2$ L) at temperatures between 30 and 140 °C. Experiments performed with a slight H_2 back pressure (∼2 bar) showed similar results. In the temperature range 60–140 °C the fractional decomposition curves exhibit a clear sigmoidal shape with distinct induction, acceleratory and decay periods as shown in Fig. 4. This shape is indicative of an autocatalytic reaction, typical of solid-state decomposition. An analysis of the fractional decomposition curves using the second and third order Avrami–Erofeyev equations [13,14] (60–140 °C) suggests that the rate of H_2 evolution is limited by nucleation and growth of the aluminum phase [6]. The activation energies and rate constants for the AlH_3 polymorphs are listed elsewhere [6,15]. At lower

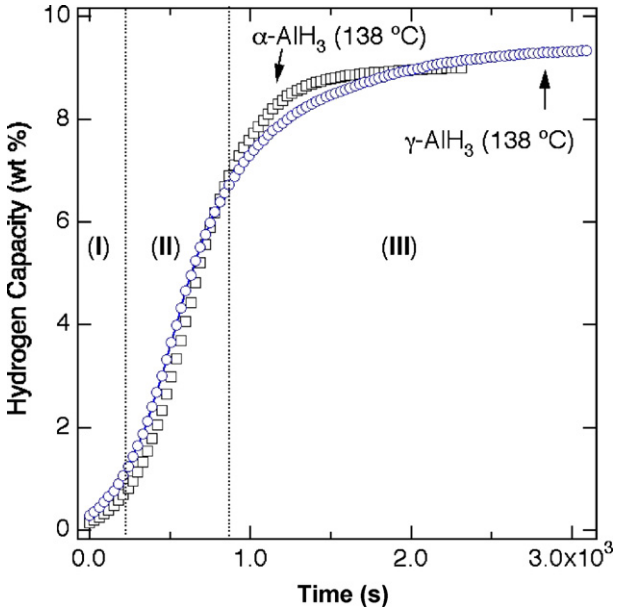

Fig. 4. High temperature isothermal decomposition curves from α and γ-AlH_3 starting materials at 138 °C showing (I) induction period (II) acceleratory period, and (III) decay period.

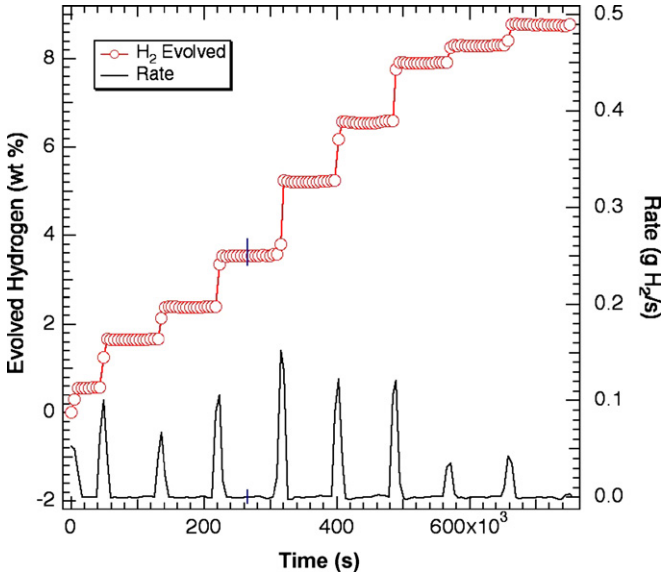

Fig. 6. Decomposition of α-AlH_3 by intermittent heating (90 °C) and cooling (23 °C) showing the total amount of H_2 evolved and the rate. The H_2 rate was determined from the first derivative of the evolved H_2 using 100 kg AlH_3. The markers at 270×10^3 s indicate a two-day break in the data set where the sample sat idle at 23 °C.

temperatures (∼30 °C) the decomposition curves appear to loose their sigmoidal shape and develop a more linear character as shown in Fig. 5. This could be indicative of a different, low temperature rate-limiting step, such as the formation of molecular hydrogen (H_2) at the surface.

Decomposition of α-AlH_3 was also investigated by intermittent heating and cooling at 90 and 23 °C, respectively. The plot in Fig. 6 shows the total H_2 evolved (upper trace) and the first derivative of the total H_2 evolved (lower trace), which corresponds to the H_2 evolution rate for 100 kg of material. The rate measured in the second decomposition step (50×10^3 s) is slightly larger than in the subsequent step due to a small overshoot in temperature (∼10 °C). However, the general trend shown in Fig. 6 is an increasing H_2 evolution rate up to ∼5 wt% evolved H_2 followed by a slow decline. This behavior is similar to that observed for the continuous decomposition of α-AlH_3 (Fig. 4). The reaction rate can be slowed and even stopped by decreasing the sample temperature. Therefore, the full spectrum of H_2 evolution rates (e.g. 0.0–1.0 gH_2/s) can likely be obtained with a 100 kg α-AlH_3 variable temperature hydride bed where $23 \leq T \leq 115$ °C.

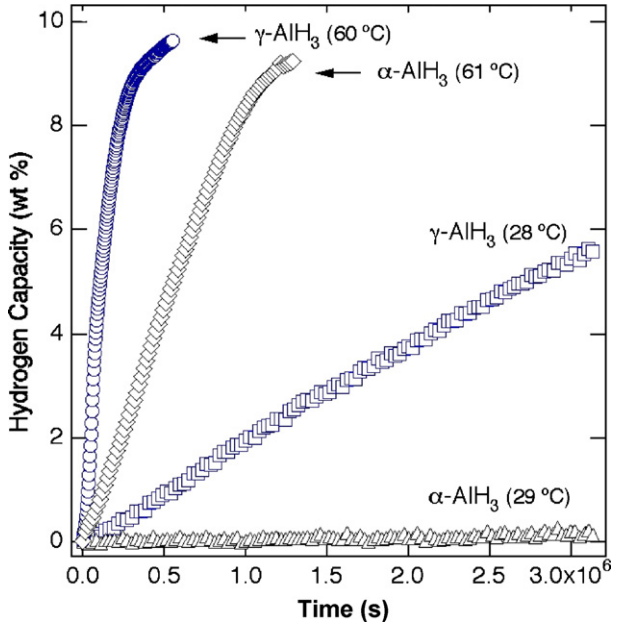

Fig. 5. Low temperature isothermal decomposition curves from α and γ-AlH_3.

Fig. 7 shows a plot of H_2 evolution rates for 100 kg of freshly prepared α and γ-AlH_3 and stabilized α-AlH_3 [15] determined from the "acceleratory" region of the fractional decomposition curves (90% of total). At temperatures greater than ∼100 °C, the H_2 evolution rates are similar for the small crystallites of α and γ-AlH_3. At high temperature, γ-AlH_3 undergoes a rapid transformation to the α phase and therefore, the H_2 evolution rate is governed by the decomposition of the α phase. At 115 °C the small crystallites of undoped α and γ-AlH_3 release H_2 at a rate of 1 gH_2/s (DOE full flow target for a 50 kW fuel cell).

At temperatures less than 100 °C, the H_2 evolution rates for γ-AlH_3 are much more rapid than the α phase, as shown in Fig. 7. This could be partially attributed to microstructural differences between the two phases. The γ phase material exhibited a larger surface area, which could explain the greater H_2 rates especially if the low temperature kinetics were limited by the formation of molecular H_2 at the surface. The rate differences could also be attributed to the low temperature decomposition pathway of the γ phase, which tends to go directly to the elements (γ-$AlH_3 \rightarrow Al + 3/2H_2$) without the intermediate α transition. The total formation enthalpy of γ-AlH_3 is approximately 30% less exothermic than that of the α phase [3] and therefore, γ-AlH_3 is less stable and has a greater driving force for decomposition.

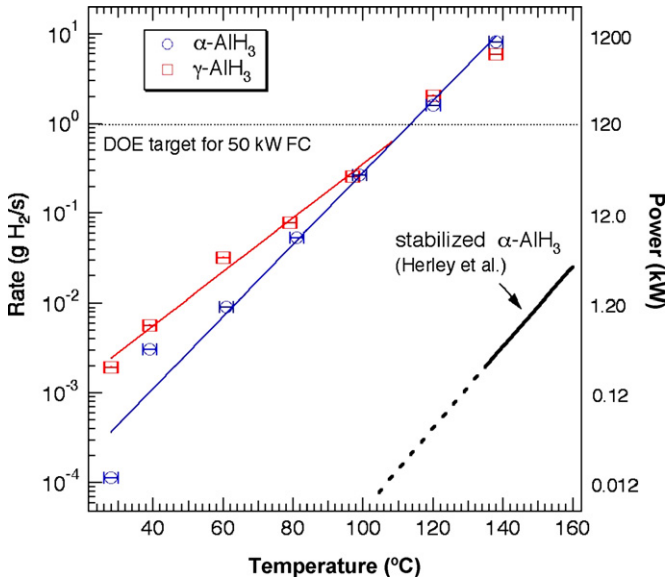

Fig. 7. Decomposition rates for freshly prepared α and γ-AlH_3 and stabilized α-AlH_3 [15] based on 100 kg of material. The dashed line represents the extrapolated rates for the stabilized α-AlH_3. The power was determined from the lower heat of combustion for H_2 (120 kJ/g).

6. Conclusion

The kinetics and thermodynamics of small crystallites of α-AlH_3 and γ-AlH_3 and a stabilized form of α-AlH_3 were investigated. We demonstrate that alane decomposition is controlled by nucleation and growth of the Al phase at temperatures 60–140 °C. Thermal decomposition of the γ polymorph typically occurs via an exothermic transition to the α phase above 100 °C with partial direct decomposition occurring at lower temperatures (<100 °C). Freshly prepared α and γ-AlH_3 exhibit similar H_2 evolution rates (0.1–0.3 gH_2/s) in the temperature range of interest (85–100 °C) for PEM fuel cell applications. Much slower rates were observed with the stabilized Dow α material (10^{-4} gH_2/s at 100 °C based on extrapolated data).

Despite similar decomposition rates above 100 °C, the γ polymorph is much less stable at low temperature (≤60 °C) and therefore, will not likely meet the durability requirements for automotive applications. Although γ-AlH_3 may be useful in low temperature, low power fuel cell applications, the α polymorph exhibits the preferred combination of low temperature stability (40 °C) with rapid H_2 evolution at moderate temperatures (100 °C). The greater durability and longer shelf life of α-AlH_3 will likely make it the preferred polymorph for automotive fuel cell applications.

Acknowledgements

This work was supported by the Department of Energy's Office of Energy Efficiency and Renewable Energy through the Metal Hydrides Center of Excellence. This manuscript has been authored by Brookhaven Science Associates, LLC under Contract No. DE-AC02-98CH1-886 with the U.S. Department of Energy. This research was partially performed at the Jet Propulsion Laboratory, which is operated by the California Institute of Technology under contract with the NASA.

References

[1] F.M. Brower, N.E. Matzek, P.F. Reigler, H.W. Rinn, C.B. Roberts, D.L. Schmidt, J.A. Snover, K. Terada, J. Am. Chem. Soc. 98 (1976) 2450.
[2] P. Claudy, B. Bonnetot, J. Etienne, G. Turck, J. Therm. Anal. 8 (1975) 255.
[3] J. Graetz, J.J. Reilly, J. Alloys Compd. 424 (2006) 262.
[4] G. Sandrock, J. Reilly, J. Graetz, W.M. Zhou, J. Johnson, J. Wegrzyn, Appl. Phys. A 80 (2005) 687.
[5] G. Sandrock, J. Reilly, J. Graetz, W.-M. Zhou, J. Johnson, J. Wegrzyn, J. Alloys Compd. 421 (2006) 185.
[6] J. Graetz, J.J. Reilly, J. Phys. Chem. B 109 (2005) 22181.
[7] N.E. Matzek, Dow Chemical Co., U.S. Patent 3,844,854 (1974).
[8] P.J. Herley, O. Christoferson, J.A. Todd, J. Solid State Chem. 35 (1980) 391.
[9] G.C. Sinke, L.C. Walker, F.L. Oetting, D.R. Stull, J. Chem. Phys. 47 (1967) 2759.
[10] J.W. Turley, H.W. Rinn, Inorg. Chem. 8 (1969) 18.
[11] J. Graetz, J. Reilly, G. Sandrock, J. Johnson, W.-M. Zhou, J. Wegrzyn, in: D. Chandra, J.J. Petrovic, R. Bautista, A. Imam (Eds.), Advanced Materials for Energy Conversion II TMS Proceedings, 2006, pp. 57–63.
[12] S.-J. Hwang, R.C. Bowman Jr., J. Graetz, J.J. Reilly, Mat. Res. Soc. Conf. Proc. 927 (2005), Paper No. 0927-EE03-03.
[13] B.V. Erofeyev, C. R. Acad. Sci. U.S.S.R. 52 (1946) 511.
[14] M. Avrami, J. Chem. Phys. 9 (1941) 177.
[15] P.J. Herley, O. Christoferson, R. Irwin, J. Phys. Chem. 85 (1981) 1887.